JOURNAL OF MATERIALS SCIENCE 10 (1975) 729–736

Hydroxyl impurity and the formation and distribution of cavities in melt-grown MgO crystals

A. BRIGGS
Materials Development Division, AERE, Harwell, Didcot, Oxon, UK

Defects causing cloudiness in melt-grown magnesium oxide crystals are identified as octahedral or cubo-octahedral cavities, with sizes in the range 10^3 to 10^4 Å, containing hydrogen at $\sim$ 400 atm pressure. A close relationship between the formation of cavities and the presence of hydroxyl impurities in the crystal is established, and a mechanism for their formation is postulated, based on the reaction of oxygen vacancies and electrons produced at the surface with V_{OH} centres in the interior of the crystal.

1. Introduction

Mechanical and physical properties of MgO crystals grown from the melt have been studied in laboratories throughout the world since the late 1950s. More recently, as part of a broad examination of the effects of reactor irradiation on ceramic materials, neutron-irradiated crystals of MgO have been studied in an attempt to identify the types and measure the concentrations of the defects produced [1]. Most of the crystals used came from two primary sources (The Norton Company and W. & C. Spicer Limited), and were produced by some variant of the arc-fusion method. The quality of the crystals produced and studied has usually been judged on their cation impurity content and optical clarity, and on these bases they can be very pure indeed. For example, some Norton or Spicer crystals can contain as little as 200 parts per million cation impurities, and be quite transparent. Other, usually larger, crystals, however, often have cloudy centres, and the cloudiness appears to be more common the lower the cation impurity content. For irradiation experiments it is advantageous to have many specimens derived from the same parent crystal, which must, therefore, be as large as possible. Since the largest crystals are often cloudy, it is important to know the causes of the cloudiness and whether it will affect the behaviour of the crystals under neutron irradiation. This paper is concerned with the nature of the cloudiness and its causes. Its effects on the irradiation properties of the material have been described by Henderson *et al.* [2]. Briggs [3] found that similar cloudiness could be produced in some, previously clear, MgO crystal specimens by annealing them in hydrogen, and that it was due to light-scattering by microscopic cavities. These formed only in crystals containing hydroxyl impurity, by the reaction of V(OH) centres with oxygen vacancies produced at the crystal surfaces. The similarity of the disposition of these cavities to that of the cloudy centres of some melt-grown crystals prompted a study of the distribution of hydroxyl impurity in the latter, and a microscopic examination of their cloudy centres.

Kirklin *et al.* [4] used a combination of infra-red absorption and electron nuclear double resonance techniques to establish conclusively that a sharp infra-red absorption peak found in MgO crystals at 3296 cm^{-1} was due to a hydroxyl vacancy associate. This peak was always associated with another at 3310 cm^{-1}, which it was suggested was also due to a hydroxyl ion, in a slightly different environment. A series of sharp peaks in the same spectral region in Spicer crystals was attributed by Glass and Searle [5] to absorption by various associates of hydroxyl ions, impurity cations and cation vacancies. A strong peak produced at $\sim$ 3700 cm^{-1} by some MgO crystals was thought by Kirklin *et al.* [4] to be due to magnesium hydroxide precipitates, and this idea was supported by Glass and Searle [5] and confirmed by the luminescence measurements of Sibley *et al.* [6]. Briggs and Bowen [7] and work to be published have shown by selected-area electron diffraction that melt-

grown MgO crystals which absorb strongly at 3698 cm^{-1} can contain $Mg(OH)_2$ precipitates. They have the same topological relationships to the MgO as those found by Garrido [8, 9] for the $Mg(OH)_2 \rightarrow MgO$ transformation. It is well-established, therefore, that the appearance of absorption bands in the region between 3290 and 3700 cm^{-1} of the infra-red spectrum for MgO indicates the presence of hydroxyl impurity, and can be used as a diagnostic tool. Moreover, using measurements of absorption coefficient and band width for the absorption bands, and assuming a value for the oscillator strength of the transitions responsible for the absorptions, it is possible, by applying the expressions developed by Smakula [10], Herring [11] and Dexter [12], to employ the absorption bands for quantitative analysis. In order to map the distribution of hydroxyl impurity in an MgO crystal, and compare it with the distribution of cloudiness, a large Spicer crystal with a cloudy central region was selected.

2. Experimental details

The crystal selected for study was, as shown in Fig. 1, approximately 50 mm long and contained a cloudy region about 30 mm long and 7 mm wide. Its length was perpendicular to the surface of the melt from which it crystallized. It was sliced perpendicular to its length with a diamond saw to give twenty-two specimens of approximately equal thickness. Each specimen was polished in hot orthophosphoric acid to produce surfaces of good optical quality, and its infra-red spectrum was measured. For this purpose the specimen, except for its central area, was masked by a matt black-painted brass plate containing a rectangular slit with dimensions 10 mm × 5 mm. The crystal exposed by the slit was placed in the sample beam, and an identical plate with a clear slit placed in the reference beam, of a Perkin-Elmer, Model 421 Dual Grating Spectrophotometer. The range 4000 to 440 cm^{-1} was scanned at a speed of 20 cm^{-1} sec^{-1} and the transmittance (%) plotted automatically against wave number (cm^{-1}) on a strip chart. For every spectrum obtained the chart was calibrated against the prominent atmospheric water peak at 3853 cm^{-1}.

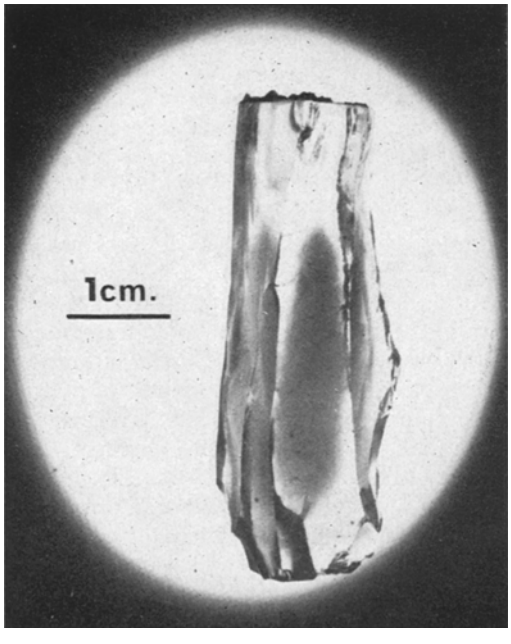

Figure 1 A Spicer MgO crystal with a central cloud of cavities.

3. Results

3.1. Hydroxyl concentration

In the OH stretching region of the spectrum most of the specimens produced eight absorption bands, which appeared at 3296, 3310, 3324, 3340, 3516, 3547, 3553 and 3698 cm^{-1}. These sharp peaks were superimposed on a very broad band extending from $\sim$ 3150 to $\sim$ 3750 cm^{-1}, and their intensities and relative intensities varied throughout the crystal. For example, spectra for specimens taken from the top, middle and bottom of the crystal are shown in Fig. 2. For all the absorption peaks, absorption coefficients were calculated from the expression

$$\mu = \frac{\ln(I_0/I)}{l}$$

where μ is the absorption coefficient (cm^{-1}), I_0 is the incident intensity, I is the transmitted intensity, l is the crystal thickness, derived from Lambert's law, taking the transmitted intensity in the absence of an absorption peak as 100% and the transmitted intensity at the centre of an absorption peak as 100% minus the peak height (%). This allows surface reflection to be neglected. Absorption coefficients for all eight absorption bands, as a function of distance from the top of the crystal, are presented in Fig. 3. On the same figure, the extent of the cloudy regions is marked, and it can be seen that its upper boundary coincides with a region of high concentration of all the species giving rise to the absorption, and its lower boundary with less well-marked maxima for most of the absorptions.

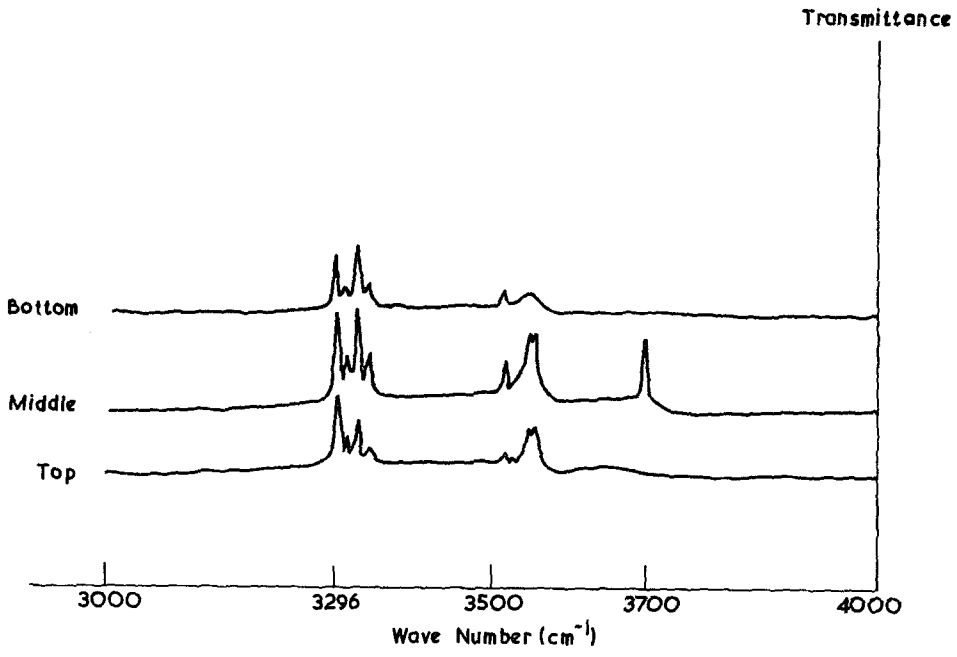

Figure 2 Infra-red spectra of slices taken from the top, middle and bottom of the crystal in Fig. 1. The traces are spread out along the transmittance axis for clarity.

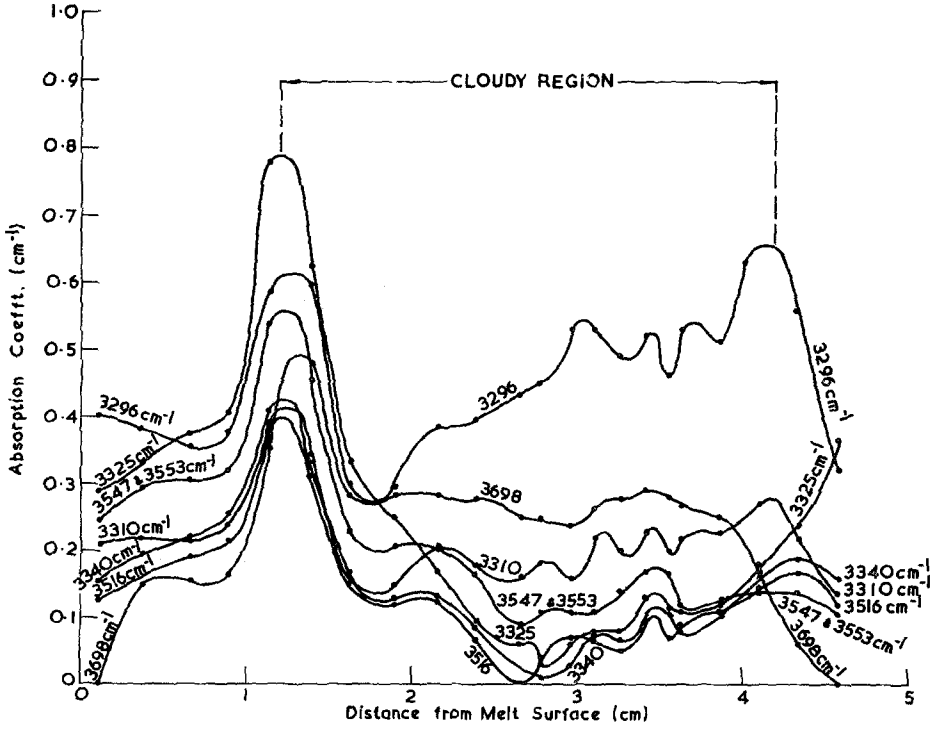

Figure 3 A plot of the absorption coefficients for eight infra-red hydroxyl bands along the length of the crystal in Fig. 1.

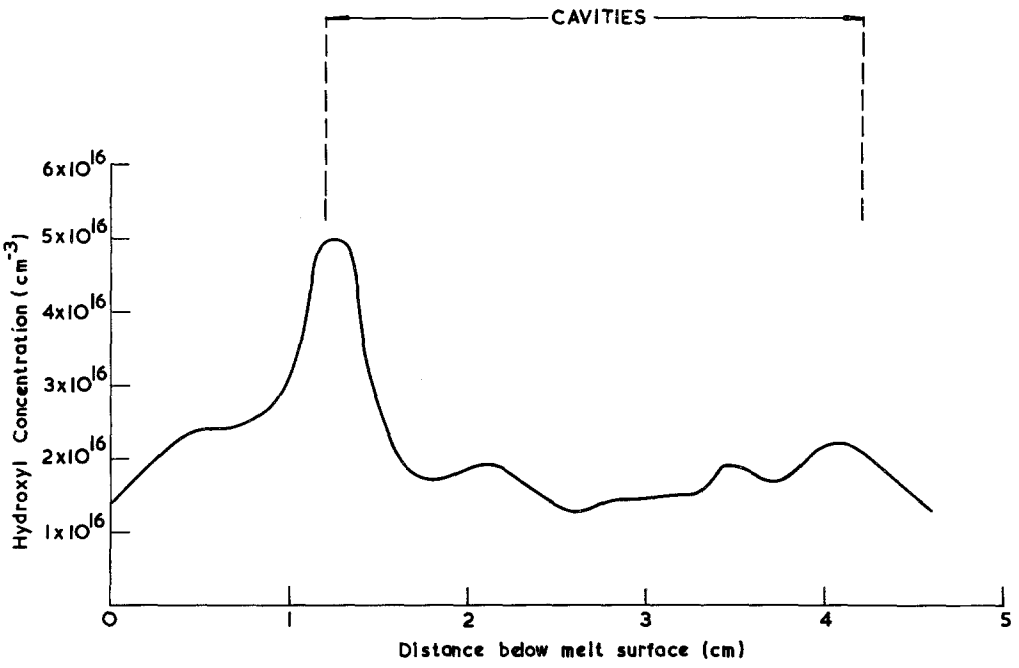

Figure 4 A plot of total hydroxyl concentration (calculated from the absorption coefficients of Fig. 3) against distance from the top of the crystal in Fig. 1.

From the absorption coefficient and band width of an absorption peak, the concentration of oscillating centres giving rise to the absorption can be calculated approximately using a modification of Smakula's dispersion theory treatment of an electronic oscillator in isolation [10], due to Herring [11] and Dexter [12], which makes a number of drastic simplifying assumptions. The outcome of the calculation is that

$$N = 1.2 \times 10^{19}\, \mu \Delta E \,\mathrm{cm}^{-3}$$

where N is the number of oscillators per cm^3, μ is the peak absorption coefficient, ΔE is the peak energy. Although the assumptions may render this equation inaccurate, it is adequate for the comparative purposes of this investigation. For all the absorption peaks the concentration of hydroxyl was computed, and the total concentration is shown as a function of depth below the melt surface in Fig. 4. On the same figure the extent of the cloudy region is marked, and it can be seen that there is a sharp fall in hydroxyl concentration on either side of its upper and lower boundaries.

3.2. Cloudiness

Ultramicroscopy showed the cloudiness to be due to light scattering by defects, < 10 μm diameter, that were almost invariably associated with sub-grain boundaries or tangled dislocation networks, as shown in Fig. 5. Shadowed surface replicas, taken from specimens cleaved through the cloudy region, and examined by transmission electron microscopy, proved that the defects were cavities, and indicated that they had a cubo-octahedral crystalline habit. Optical microscope observation of the same cleaved

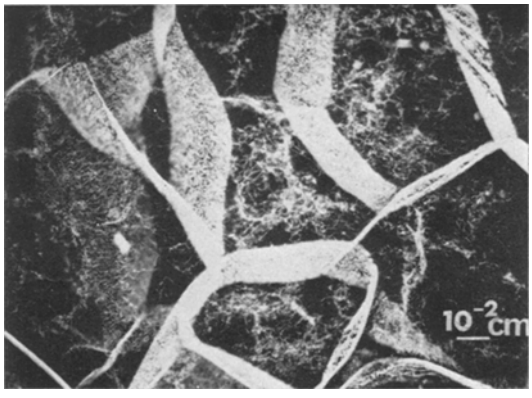

Figure 5 An ultramicroscope photograph of defects on sub-grain boundaries and tangled dislocations in crystals as-grown.

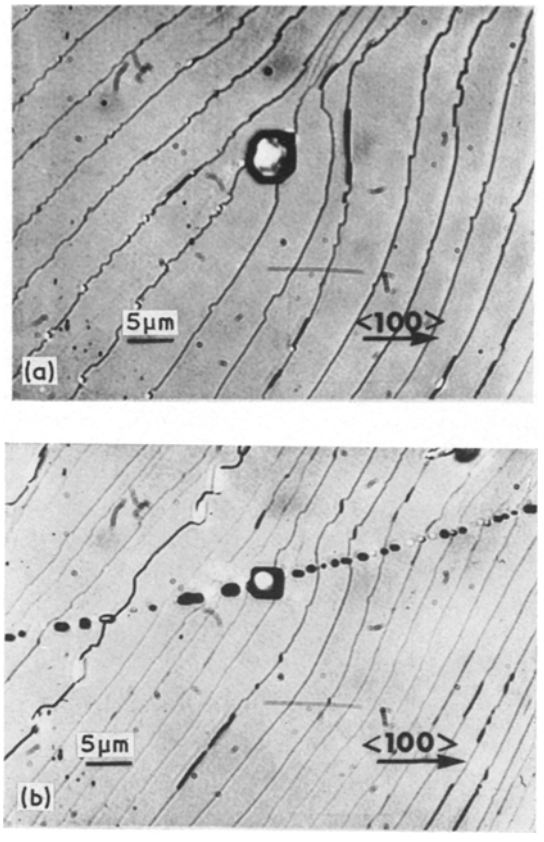

Figure 6 (a) A cavity with ⟨100⟩ and ⟨110⟩ sides, exposed on a cleaved surface. (b) Cavities on a sub-grain boundary, exposed on a cleaved surface.

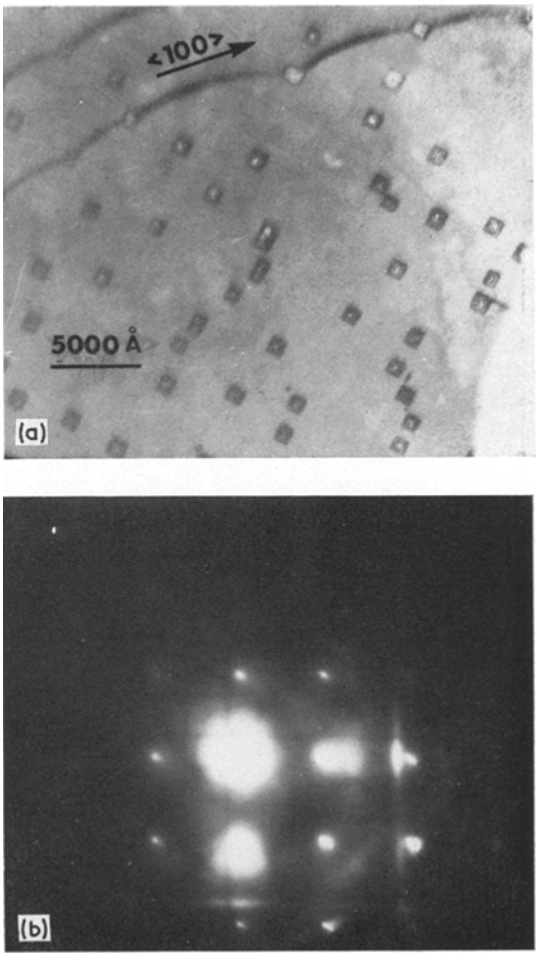

Figure 7 (a) Cavities in a crystal as-grown, seen by transmission electron-microscopy. (b) A selected-area diffraction pattern from the area in (a).

surfaces showed the larger cavities to have ⟨100⟩ and ⟨110⟩ edges in the plane of the cleavage (Fig. 6). This is consistent with the cavities having {100} and {111} facets. Cavities less than ~ 1 μm diameter were best studied by transmission electron microscopy of thin foils, which showed that they all projected in the (100) plane as squares with ⟨110⟩ edges. In the smallest of these cavities, which remained wholly within the foil, as shown in Fig. 7a, thickness fringes could be seen, and hence their depths could be calculated.

The reflection producing the thickness fringes was known to be (200) from a diffraction pattern taken from the same area (Fig. 7b), which is rotated ~ 40° from the micrograph by the different electron optical arrangement. The extinction distance for this reflection is 460 Å [13]. The group of cavities in Fig. 7 all have {111} facets, and their depths vary from 1840 to 2760 Å (since they are symmetrical octahedra, thickness fringes produced by their upper and lower halves are superimposed, so that the number of fringes must be doubled).

3.3. The pressure and nature of gas in the cavities

Whilst cloudy crystals were being chemically polished, for the infra-red absorption measurements described above, streams of bubbles were noticed emanating from them. Closer examination under an optical microscope showed the bubbles to be coming from systems of connected cavities along sub-grain boundaries. It was further noticed that, whenever an isolated cavity was breached by the hot acid, it emitted a bubble

of gas which remained attached to the crystal surface at the site of the cavity. In order to estimate the pressure of gas in the cavities they were photographed, before and after bubbles had emerged from them, with the crystal immersed in acid in both cases to avoid refractive index errors when comparing their sizes. From measurements on the photographs the volumes of cavities and bubbles were calculated, and from the volume ratios the gas pressures were obtained. Cavity and bubble volumes and the gas pressures are shown in Table I. The mean gas pressure in the cavities was $\sim$ 800 atm, including the very high value for cavity number 7. If this result is regarded as spurious and ignored, the mean value is 440 atm, which is very close to the figure found by Briggs [3] for the pressure of hydrogen gas in cavities produced in MgO crystals by annealing them in reducing atmospheres.

TABLE I Gas pressure in cavities in crystals as-grown

Cavity number	Cavity volume (cm^3)	Bubble volume (cm^3)	Cavity pressure (atm)
1	1.3×10^{-11}	3.8×10^{-9}	300
2	9×10^{-12}	1.5×10^{-9}	160
3	3.1×10^{-11}	2.0×10^{-9}	65
4	4×10^{-12}	3.5×10^{-9}	970
5	1.4×10^{-12}	4.9×10^{-10}	350
6	1.4×10^{-12}	7.0×10^{-10}	500
7	9×10^{-13}	3.5×10^{-10}	3800
8	9×10^{-13}	7.0×10^{-10}	770
9	2.6×10^{-12}	6.0×10^{-10}	230

An attempt to analyse the gas in the cavities by crushing the crystals in an attachment to a mass-spectrometer was not successful, probably because the crushing did not open up enough cavities to release sufficient gas to be detected. Accordingly, an experiment was tried in which all the gas was released by dissolving the crystal. Two glass breaker-seal tubes were prepared, one containing a cloudy crystal specimen and 1 ml orthophosphoric acid, and the other, as a control, containing 1 ml acid only. The ends of the tubes containing the acid were evacuated and sealed whilst the acid was frozen by immersion in liquid nitrogen. The specimen was then dissolved by heating the acid at 100° C (the control tube receiving the same treatment) and both tubes were attached, via a glass manifold, to the vacuum system of the mass-spectrometer. They were evacuated to a pressure $\sim 10^{-6}$ Torr, the acid again frozen, and the seals broken in turn by magnetically raising and dropping glass-encapsulated steel slugs. The mass-spectrometer detected an increase in mass 2 to $\sim$ 50% above background level for the specimen tube, and about 10% above background for the control. Similar experiments with clear crystal gave a similar result to the control. It is concluded, therefore, that cavities in cloudy as-grown MgO crystals contain hydrogen.

4. Discussion

Briggs [3] has proposed a detailed mechanism for the formation of hydrogen-filled cavities in MgO crystals annealed in flowing reducing atmospheres. The essential steps in the mechanism are:

(a) removal of oxygen ions or hydroxyl ions from the surface creates oxygen vacancies plus electrons according to the reactions,

(i) $H_2 + MgO \rightarrow H_2O + Mg + \boxed{O} + 2e$

(ii) $H + Mg{-}OH \rightarrow H_2O + Mg + \boxed{O} + e$

$\boxed{O}$ is an oxygen vacancy carrying an effective double positive charge, e is an electron;

(b) oxygen vacancies and electrons diffuse into the crystal, possibly in association;

(c) Within the crystal, oxygen vacancies and electrons combine with hydroxyl/magnesium vacancy complexes according to the reaction,

$$\boxed{Mg} - OH^- + \boxed{O} + e \rightarrow \boxed{Mg}\,\boxed{O} + H + O^{2-}$$

$\boxed{Mg}\,\boxed{O}$ is a divacancy

A divacancy containing a hydrogen atom is formed, which diffuses and condenses with similar entities to form a cavity nucleus containing hydrogen gas molecules, under 400 atm pressure.

In the carbon-arc fusion process by which the crystals used in the present study were prepared, the conditions allow a cavity formation mechanism to proceed which is broadly similar in principle to that described above, but different in detail. A description of the mechanism hinges on details of the crystal-growing process, an account of which follows.

(1) MgO powder, which normally contains some magnesium hydroxide, some bulk and surface hydroxyl, and some adsorbed water, is packed around graphite electrodes in a water-cooled furnace.

(2) An arc is struck between the electrodes, heats the powder, drives adsorbed water from the

hotter to the cooler regions, and decomposes $Mg(OH)_2$.

(3) Powder near the arc sinters, then melts, and forms a pool at the bottom of a domed cavern, which grows by wall-melting.

(4) Various chemical reactions occur, to produce a mixture of gases under moderate pressure:

(i) adsorbed OH → water vapour
(ii) $C + H_2O \rightarrow CO + H_2$
(iii) $2C + O_2 \rightarrow 2\,CO$
(iv) $MgO + C \rightarrow Mg + CO$.

This mixture constitutes a reducing atmosphere, which becomes dynamic when the gas pressure blows a hole in the roof of the cavern, usually near an electrode, and the gases are vented. Gas continues to escape throughout a run.

(5) The arc is switched off, the melt cools at a rapid rate, and forms a mass of columnar crystals.

Although most of the hydroxyl, usually present as H_2O, $Mg(OH)_2$ or adsorbed OH, is driven off, decomposed or reacted, an equilibrium concentration of OH^- ions remains in solution in the molten MgO, and is incorporated in crystals when the melt solidifies. The newly-solidified MgO also contains the equilibrium number of vacancies appropriate to its temperature, in addition to vacancies compensating for altervalent impurity ions. The presence of magnesium vacancies and OH^- ions in the crystal, and the reducing atmosphere above it, allows the formation of cavities, and liberation of hydrogen in them, to proceed by a mechanism similar to the one outlined above, soon after solidification. Hydrogen/divacancy agglomerates formed close to the surface are able to diffuse out, and this accounts for the absence of cavities in the outer regions of the crystals. In these regions, and in crystals containing smaller hydroxyl concentrations, or more cation impurities, as the temperature continues to fall, the planar agglomerates of vacancies, hydroxyl ions and impurity cations postulated by Briggs [3] may be formed. Meanwhile the rapid cooling produces strains that introduce dislocations, which migrate by glide and climb to form subgrain boundaries and dislocation tangles. These serve as nucleating centres for both cavities and the agglomerate sheets. When all the available cation impurities and vacancies have formed complexes with OH^- ions, the remaining hydroxyl impurity is able to enter the MgO lattice as free, substitutional OH^- ions. (Stoebe [14] has shown for the case of lithium fluoride that OH^- ions will first form complexes with impurities and vacancies, and will not, until all these are used up, enter the lattice as free substitutional OH^- ions.) The OH^- complex distribution may be modified by diffusion to the surface or to the cavities that formed first. There hydrogen may be evolved by a mechanism proposed by Freund and Gentsch [15], accounting for the hydroxyl complex distribution shown in Fig. 3. In crystals containing more hydroxyl than is needed to exhaust the supply of vacancies for complex formation and satisfy the equilibrium solubility requirements, magnesium hydroxide precipitates may form. The infra-red absorption results show that the distributions of brucite* precipitates and hydroxyl complexes are similar (except that no brucite is found very close to the surface), so it is possible that the brucite nucleates on the complex agglomerates. The vacancies of a nearby complex agglomerate might facilitate the crystallographic re-arrangements necessary for the transformation of MgO to brucite.

*Magnesium hydroxide crystal.

5. Conclusions

(1) The defects causing some melt-grown MgO crystals to appear cloudy are octahedral cavities with {111} facets or cubo-octahedral cavities with {111} and {100} facets.

(2) The cavities contain hydrogen gas under 400 atm pressure.

(3) The distribution of the cavities is closely related to the distribution of hydroxyl impurities.

(4) The gas-filled cavities form by a mechanism which involves the reaction of oxygen vacancies and electrons, produced by a reduction reaction at the surface, with magnesium vacancy/OH^- complexes in the interior of the crystal, followed by agglomeration of the resulting divacancies.

References

1. B. HENDERSON and D. H. BOWEN, *J. Phys. C. Sol. Stat. Phys.* **4** (1971) 1487.
2. B. HENDERSON, D. H. BOWEN, A. BRIGGS and R. D. KING, *ibid* **4** (1971) 1496.
3. A. BRIGGS, *J. Mater. Sci.* **10** (1975) 737.
4. P. W. KIRKLIN, P. AUZINS and J. E. WERTZ, *J. Phys. Chem. Solids* **26** (1965) 1067.
5. A. M. GLASS and T. M. SEARLE, *J. Chem. Phys.* **46** (1967) 2092.
6. W. A. SIBLEY, C. M. NELSON and Y. CHEN, *ibid* **48** (1968) 4582.

7. A. BRIGGS and D. H. BOWEN, "Mass Transport in Oxides", National Bur. Stand. Special Publ. 296 (1968) p. 103.
8. J. GARRIDO, *Ion. Rev. Espan. Quim. Aplic.* **11** (1951) 206.
9. *Idem, ibid* **11** (1951) 453.
10. A. SMAKULA, *Z. Phys.* **59** (1930) 603.
11. C. HERRING, "Proceedings of the Conference on Photoconductivity" (Wiley, New York, 1955).
12. D. L. DEXTER, *Phys. Rev.* **101** (1956) 48.
13. P. B. HIRSCH, A. HOWIE and M. J. WHELAN, *Phil. Trans. Roy. Soc. A* **252** (1960) 499.
14. T. G. STOEBE, *J. Phys. Chem. Solids* **28** (1967) 1375.
15. F. FREUND and H. GENTSCH, *Ber. Deutsch. Keram. Ges.* **44** (1967) 51.

Received 11 November and accepted 25 November 1974.